Phased Array Radio Navigation System on UAVs: Real-Time Implementation of In-flight Calibration ⋆

Mika Okuhara Torleiv H. Bryne Kristoffer Gryte Tor Arne Johansen

Department of Engineering Cybernetics, The Norwegian University of Science and Technology, Trondheim, Norway. (email: mika.okuhara@ntnu.no, torleiv.h.bryne@ntnu.no, kristoffer.gryte@ntnu.no, tor.arne.johansen@ntnu.no)

Abstract: Unmanned aerial vehicles (UAV) require an alternative positioning system to the global navigation satellite systems (GNSS) for safety-critical operations since GNSS is prone to unintentional or malicious electromagnetic interference. As a possible redundant positioning solution independent of GNSS, the phased array radio system (PARS) has proved its potential as a local navigation system for UAVs. Previous work suggested an automatic calibration algorithm to estimate the precise PARS ground antenna orientation to improve PARS positioning accuracy. This algorithm was then integrated with PARS- and barometer-aided inertial navigation system (INS) based on multiplicative extended Kalman filter (MEKF) to enable in-flight calibration when GNSS is available. This paper presents the implementation of the previously suggested aided-INS with in-flight calibration mode for real-time operation.

Keywords: Unmanned aerial vehicles (UAV), Phased array radio system (PARS), Inertial navigation system (INS), Multiplicative extended Kalman filter (MEKF)

1. INTRODUCTION

Due to the advantages of high precision positioning, global coverage, lightweight receiver, and low cost, the global navigation satellite systems (GNSS) has been used as a primary positioning system for unmanned aerial vehicles (UAV). Integrated navigation systems using GNSS measurement to aid inertial navigation systems (INSs) are particularly useful considering the high precision, high accuracy, and high bandwidth position estimate at a high rate being provided. However, positioning relying on only GNSS has safety issues due to the low signal-to-noise ratio (SNR) which makes GNSS prone to interference and malicious attacks such as jamming (Pinker and Smith, 1999; Humphreys, 2017) and spoofing (Kerns et al., 2014; Humphreys, 2017). For this reason, it is important to establish a redundant positioning system for safety-critical operations.

One of the promising solutions is the phased array radio system (PARS). Although PARS is primarily designed as a high-bandwidth communication link, it can also be used as a local navigation system by finding a position relative to a ground antenna. The much higher SNR and strong encryption can compensate for the cyber-security issue of GNSS. The disadvantage of PARS is the need for a radio link and the lower accuracy than GNSS. Particularly, the precision of ground antenna mounting orientation has a great impact on the accuracy of positioning estimate, as PARS measures the position in the local frame fixed on the antenna.

Seeking the possibility of GNSS-free navigation, PARS as a positioning solution for UAVs has been under research for several years. In the early works, Albrektsen et al. (2017, 2018a,b) have done PARS data collection, and presented PARS-aided INS using a non-linear observer. More recent work (Gryte et al., 2019; Gryte et al., 2020) has implemented PARS-aided INS using the multiplicative extended Kalman filter (MEKF). The change from non-linear observer to MEKF was motivated by the access to cross-covariance between all states being advantageous when fusing inertial and PARS measurements. In the previous work, the ground antenna orientation was measured manually by a compass, or by aligning PARS with GNSS measurements by manually adjusting the PARS orientation, even though high precision in the ground antenna orientation is required to obtain high accuracy in position estimate. Hence, an automatic calibration algorithm to estimate the ground antenna orientation was suggested in Okuhara et al. (2021), and the algorithm was integrated with aided-INS to enable in-flight calibration in Okuhara et al. (2022). Moreover, Okuhara et al. (2022) resolved the navigation dynamics (i.e. INS equations) in the Earth Centred Earth Fixed (ECEF) frame, while the previous work used the local North East Down (NED) frame.

⋆ This research was funded by the Research Council of Norway, Radionor Communications and Andøya Space through the BIA program's UAAFA project number 309370, and through the Centre for Autonomous Marine Operations and Systems, project number 223254.

1.1 Main contribution

In this paper, the previously presented in-flight calibration algorithm in Okuhara et al. (2022) was implemented in the DUNE unified navigation environment (Pinto et al., 2013) for real-time operation. This implementation was verified using replay data collected from field tests and validated by comparing the result with RTK GNSS measurement and Pixhawk autopilot solution as ground truth.

1.2 Organization

Starting with mathematical preliminaries in Sec. 2, multiple positioning techniques (including PARS) are presented in Sec. 3. Sec. 4 explains the formulation of the navigation system including MEKF-based aided-INS with in-flight calibration algorithm for PARS ground antenna based on the mathematical preliminaries and the positioning techniques presented in previous sections. Using the replay data obtained from field tests, the suggested navigation system is validated and discussed in Sec. 5.

2. PRELIMINARIES

This section describes mathematical preliminaries before presenting the positioning techniques and the navigation system.

2.1 Notations

Coordinate frames are expressed as $\{\cdot\}$, while $\boldsymbol{z}_{bc}^{a} \in \mathbb{R}^3$ denotes a vector $\boldsymbol{z}$ from frame $\{b\}$ to $\{c\}$, resolved in $\{a\}$. $\boldsymbol{S}(\cdot) \in SS(3)$ denotes a skew symmetric matrix such that $\boldsymbol{S}(\boldsymbol{z}_1)\boldsymbol{z}_2 = \boldsymbol{z}_1 \times \boldsymbol{z}_2$. The Euclidean vector norm is denoted $\|\cdot\|_2$, and the transpose of a vector or a matrix is denoted $(\cdot)^\intercal$. The $n \times n$ identity matrix is denoted $\boldsymbol{I}_n$. In addition, $\mathrm{diag}(\star_1, ..., \star_n)$ represents a diagonal matrix which places the n arguments diagonally. Error variables are represented with $\delta\star$, where $\star$ is a variable placeholder. Zero-mean Gaussian noise is denoted $\varepsilon_\star \sim \mathcal{N}(0, \sigma_\star^2)$ with standard deviation $\sigma_\star$, and $\mathbb{E}[\cdot]$ denotes the expected value.

2.2 Attitude representations and relationships

In this paper, attitudes are represented as unit quaternions, using the Hamiltonian representation. For a rotation from a frame $\{a\}$ to another frame $\{b\}$, the unit quaternion is given as

$$\boldsymbol{q}_a^b = (q_s,\ \boldsymbol{q}_v)^\intercal . \tag{1}$$

The unit quaternion contains the *real* or *scalar* part referred as q_s, and the *imaginary* or *vector* part as $\boldsymbol{q}_v = (q_x, q_y, q_z)^\intercal$. The rotation from $\{a\}$ to $\{b\}$ can also be represented as the rotation matrix, $\boldsymbol{R}_{ba} \in SO(3)$. The quaternion can be related to the rotation matrix by

$$\boldsymbol{R}_{ba}(\boldsymbol{q}_a^b) = \left(q_s^2 - \boldsymbol{q}_v^\intercal \boldsymbol{q}_v\right)\boldsymbol{I}_3 + 2q_s\boldsymbol{S}(\boldsymbol{q}_v) + 2\boldsymbol{q}_v\boldsymbol{q}_v^\intercal \tag{2}$$

as given in e.g. (Markley, 2003, Eq. (4)), (Solà, 2017, Eq. (117)) and (Farrell, 2008, App. D.2).

The three-dimensional attitude error, $\delta\boldsymbol{a}$ used in the MEKF state vector is parameterized using four times the Modified Rodrigues Parameters (MRPs), $\delta\boldsymbol{a}_{\mathrm{mrp}}$

$$\delta\boldsymbol{a} = 4\delta\boldsymbol{a}_{\mathrm{mrp}} = 4\frac{\delta\boldsymbol{q}_v}{1 + \delta q_s}, \tag{3}$$

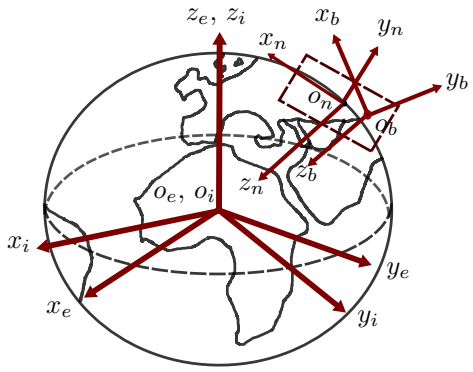

Fig. 1. Definitions of the ECI, the ECEF, the NED and the BODY coordinate frames

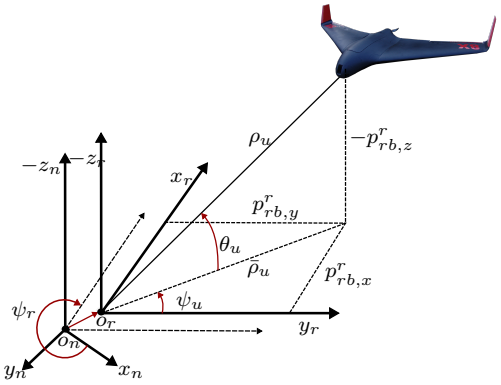

Fig. 2. Range/azimuth/elevation measurements in PARS. ψ_r denotes the yaw angle between $\{n_j\}$ and $\{r_j\}$ (the index j is omitted in the figure). Range is represented with ρ_u and the azimuth and elevation angles are represented with ψ_u and θ_u.

and the error quaternion can be computed from $\delta\boldsymbol{a}$ using

$$\delta\boldsymbol{q}(\delta\boldsymbol{a}) = \frac{1}{16 + a_p^2}\begin{pmatrix} 16 - a_p^2 \\ 8\delta\boldsymbol{a} \end{pmatrix} \tag{4}$$

where $a_p = \|\delta\boldsymbol{a}\|_2$, as given in Markley (2003). Additionally, the Euler angles (roll, pitch and yaw) are represented as

$$\boldsymbol{\Theta} = (\phi,\ \theta,\ \psi)^\intercal . \tag{5}$$

2.3 Coordinate frames

This paper considers $4 + 2m$ coordinate frames: the Earth Centered Inertial (ECI) frame, the Earth Centered Earth Fixed (ECEF) frame, the North East Down (NED) frame, the BODY reference frame of the UAV, the local PARS coordinate frames, and the local NED frames, denoted $\{i\}$, $\{e\}$, $\{n\}$, $\{b\}$, $\{r_j\}$ and $\{n_j\}$ respectively, where m is the number of PARS ground antennas in use, and $j = 1, \cdots, m$ is the PARS index. Please note that $\{n\}$ and $\{n_j\}$ are different frames, where the origin of $\{n\}$ is on the UAV while the origin of $\{n_j\}$ in on the PARS ground antenna. Fig. 1 illustrates the first four frames, and Fig. 2 shows the remaining local frames with the geometry of the UAV position.

In this paper, a single PARS ground antenna was used (i.e. $m = 1$), and therefore the index j is omitted for convenience (i.e. $\{n\}$-frame in the rest of this paper means $\{n_j\}$-frame.). The frames $\{n_j\}$ and $\{r_j\}$ have a coincided

origin (i.e. $O_{n_j} = O_{r_j}$), and the rotation between these frames expresses the PARS ground radio orientation (i.e. $\boldsymbol{R}_{nr}$ or $\boldsymbol{q}_r^n$).

This paper resolves the navigation equations in the $\{e\}$-frame, while the previous implementation Gryte et al. (2019); Gryte et al. (2020) used the $\{n_j\}$-frame.

3. POSITIONING

This section presents positioning techniques (i.e. INS and aiding measurements) used to formulate the navigation system and the PARS calibration described in the subsequent section.

3.1 Inertial Navigation System

INS obtains the UAV position by integrating specific force and angular rate measurements provided by an inertial measurement unit (IMU).

Inertial measurement unit. A simplified measurement model of IMU, providing specific force ($\boldsymbol{f}^b_{\text{IMU}}$) and angular rate ($\boldsymbol{\omega}^b_{\text{IMU}}$), is given as

$$\boldsymbol{f}^b_{\text{IMU}} = \boldsymbol{f}^b_{ib} + \boldsymbol{b}^b_{acc} + \boldsymbol{\varepsilon}^b_{acc} \tag{6}$$

$$\boldsymbol{\omega}^b_{\text{IMU}} = \boldsymbol{\omega}^b_{ib} + \boldsymbol{b}^b_{ars} + \boldsymbol{\varepsilon}^b_{ars} \tag{7}$$

where $\boldsymbol{b}^b_\star$ is the accelerometer (ACC) and the angular rate sensor (ARS) biases. The biases are modeled as Gauss-Markov processes

$$\dot{\boldsymbol{b}}^b_\star = -\boldsymbol{T}_\star^{-1}\boldsymbol{b}^b_\star + \boldsymbol{\varepsilon}_{b_\star} \tag{8}$$

where $\boldsymbol{T}_\star$ represents the time constant matrices of the two processes and $\boldsymbol{\varepsilon}_{b_\star} \sim \mathcal{N}(0, \sigma^2_\star)$.

Strapdown Equations. The position and velocity of the UAV relative to the $\{e\}$-frame are denoted as $\boldsymbol{p}^e_{eb} \in \mathbb{R}^3$ and $\boldsymbol{v}^e_{eb} \in \mathbb{R}^3$. The attitude and the angular rate of the UAV relative to the $\{e\}$-frame are given as the unit quaternion $\boldsymbol{q}^e_b$ and as $\boldsymbol{\omega}^b_{eb} = \boldsymbol{\omega}^b_{ib} - \boldsymbol{R}_{eb}{}^\intercal \boldsymbol{\omega}^e_{ie} \in \mathbb{R}^3$, where $\boldsymbol{\omega}^e_{ie} = (0, 0, \omega_{ie})^\intercal$ is the angular rate of the Earth rotation. The gravity vector $\boldsymbol{g}^e_b(\boldsymbol{p}^e_{eb})$ can be calculated from the position of the UAV (Groves, 2013, Ch. 2.4.6). The strapdown equation given relative to ECEF follows:

$$\dot{\boldsymbol{p}}^e_{eb} = \boldsymbol{v}^e_{eb} \tag{9}$$

$$\dot{\boldsymbol{v}}^e_{eb} = -2\boldsymbol{S}(\boldsymbol{\omega}^e_{ie})\boldsymbol{v}^e_{eb} + \boldsymbol{R}_{eb}\boldsymbol{f}^b_{ib} + \boldsymbol{g}^e_b(\boldsymbol{p}^e_{eb}) \tag{10}$$

$$\dot{\boldsymbol{q}}^e_b = \frac{1}{2}\boldsymbol{q}^e_b \otimes \boldsymbol{\omega}^b_{ib} - \frac{1}{2}\boldsymbol{q}^e_b \otimes \boldsymbol{\omega}^e_{ie} \tag{11}$$

3.2 Real-time kinematic GNSS

To provide the ground truth of the UAV position, real-time kinematic positioning (RTK) GNSS was used in this paper due to its high accuracy.

3.3 Phased Array Radio System positioning

PARS measures a geometric range ρ_u, the azimuth angle ψ_u and elevation angle θ_u of the UAV in the $\{r\}$-frame to determine its position, as shown in Fig. 2. Including measurement noise, the actual measurements are represented as

$$\rho_y = \rho_u + \varepsilon_\rho, \tag{12}$$

$$\psi_y = \psi_u + \varepsilon_\psi, \tag{13}$$

$$\theta_y = \theta_u + \varepsilon_\theta. \tag{14}$$

The range ρ_u, azimuth ψ_u and elevation θ_u can be related to the Cartesian UAV position in the $\{r\}$-frame using

$$\boldsymbol{p}^r_{\text{PARS}} = \begin{pmatrix} p^r_{rb,x} \\ p^r_{rb,y} \\ p^r_{rb,z} \end{pmatrix} = \begin{pmatrix} \rho_u \cos(\psi_u)\cos(\theta_u) \\ \rho_u \sin(\psi_u)\cos(\theta_u) \\ -\rho_u \sin(\theta_u)) \end{pmatrix}. \tag{15}$$

3.4 Barometer

A barometer measures the air pressure and then uses a standard atmospheric model to determine the height. Barometer-based altitude measurement was used for vertical aiding to mitigate errors in PARS elevation angle measurements, as mentioned in Sec 4.2.2.

4. NAVIGATION SYSTEM

The navigation system implemented in this paper is essentially an aided-INS presented in Okuhara et al. (2022). INS propagates the system dynamics using the IMU measurements (in Sec. 3.1), and MEKF applies corrections to the INS states (i.e. nominal states in Sec. 4.1) using the aiding measurements presented in Sections 3.2 - 3.4. For more details about MEKF, please see Okuhara et al. (2022, 2021); Gryte et al. (2020).

Fundamentally, the INS is aided using two modes. The first mode performs the calibration of the ground antenna orientation using the algorithm presented in Okuhara et al. (2021). Here, both PARS and GNSS aid the INS, and the calibration algorithm uses the position estimates from the GNSS-aided INS as ground truth. The second mode is PARS and barometer-aided INS, which is the normal GNSS-free navigation. Sec. 4.2 and Sec. 4.3 describe mode 1 and mode 2, respectively.

4.1 Navigation system model

Nominal system kinematics. The nominal state estimate (i.e. the state vector of the INS) is given as

$$\hat{\boldsymbol{x}} = (\hat{\boldsymbol{p}}^e_{eb},\ \hat{\boldsymbol{v}}^e_{eb},\ \hat{\boldsymbol{q}}^e_b,\ \hat{\boldsymbol{b}}^b_{\text{acc}},\ \hat{\boldsymbol{b}}^b_{\text{ars}},\ \boldsymbol{q}^n_r)^\intercal \in \mathbb{R}^{1\times 20}. \tag{16}$$

The nominal state is propagated using the following kinematic model based on the IMU measurement model and discretized strapdown equations presented in Sec. 3.1:

$$\hat{\boldsymbol{\omega}}^b_{eb} = \boldsymbol{\omega}^b_{\text{IMU}} - \hat{\boldsymbol{b}}^b_{\text{ars}} - \hat{\boldsymbol{R}}^\intercal_{eb}\boldsymbol{\omega}^e_{ie} \tag{17}$$

$$\Delta\boldsymbol{q}^e_b = \begin{pmatrix} \cos\left(\frac{T_s}{2}\cdot\|\hat{\boldsymbol{\omega}}^b_{eb}\|_2\right) \\ \sin\left(\frac{T_s}{2}\cdot\|\hat{\boldsymbol{\omega}}^b_{eb}\|_2\right)\cdot\frac{\hat{\boldsymbol{\omega}}^b_{eb}}{\|\hat{\boldsymbol{\omega}}^b_{eb}\|_2} \end{pmatrix} \tag{18}$$

$$\hat{\boldsymbol{q}}^e_b \leftarrow \hat{\boldsymbol{q}}^e_b \otimes \Delta\boldsymbol{q}^e_b \tag{19}$$

$$\hat{\boldsymbol{R}}_{eb} = \boldsymbol{R}_{eb}(\hat{\boldsymbol{q}}^e_b), \quad \text{using (2)} \tag{20}$$

$$\bar{\boldsymbol{R}}_{eb} = (\boldsymbol{R}_{eb} + \boldsymbol{R}_{eb,\text{prev}})/2 \tag{21}$$

$$\hat{\boldsymbol{f}}^b_{ib} = \boldsymbol{f}^b_{\text{IMU}} - \hat{\boldsymbol{b}}^b_{\text{acc}} \tag{22}$$

$$\hat{\boldsymbol{a}}^e_{eb} = -2\boldsymbol{S}(\boldsymbol{\omega}^e_{ie})\,\hat{\boldsymbol{v}}^e_{eb} + \bar{\boldsymbol{R}}_{eb}\hat{\boldsymbol{f}}^b_{ib} + \boldsymbol{g}^e_b \tag{23}$$

$$\hat{\boldsymbol{v}}^e_{eb} \leftarrow \hat{\boldsymbol{v}}^e_{eb} + T_s\cdot\hat{\boldsymbol{a}}^e_{eb} \tag{24}$$

$$\hat{\boldsymbol{p}}^e_{eb} \leftarrow \hat{\boldsymbol{p}}^e_{eb} + T_s\cdot\hat{\boldsymbol{v}}^e_{eb} + \frac{T_s^2}{2}\cdot\hat{\boldsymbol{a}}^e_{eb} \tag{25}$$

$$\hat{\boldsymbol{b}}^b_{\text{acc}} \leftarrow e^{-T_s\cdot\boldsymbol{T}^{-1}_{\text{acc}}}\cdot\hat{\boldsymbol{b}}^b_{\text{acc}} \tag{26}$$

$$\hat{\boldsymbol{b}}^b_{\text{ars}} \leftarrow e^{-T_s \cdot \boldsymbol{T}^{-1}_{\text{ars}}} \cdot \hat{\boldsymbol{b}}^b_{\text{ars}} \tag{27}$$

$$\boldsymbol{R}_{eb,\text{prev}} = \hat{\boldsymbol{R}}_{eb}. \tag{28}$$

similar to (Groves, 2013, Ch. 5). The derivative of $\boldsymbol{q}^n_r$ is zero, as the ground antenna is stationary.

Error-state system kinematics. The error state (i.e. the state vector of the MEKF) is given as

$$\delta\boldsymbol{x} = (\delta\boldsymbol{p}^e_{eb},\ \delta\boldsymbol{v}^e_{eb},\ \delta\boldsymbol{a}^e_b,\ \delta\boldsymbol{b}^b_{acc},\ \delta\boldsymbol{b}^b_{ars},\ \delta\boldsymbol{a}^n_r)^\intercal \in \mathbb{R}^{18}. \tag{29}$$

Please note that the 3D attitude error states $\delta\boldsymbol{a}^\star_\star$ (UAV and the ground radio) parameterized as four times MRPs rather than rotation matrices or quaternions, are used to update the INS's states when correcting the nominal state using (4). The continuous-time linearized error state system model is

$$\delta\dot{\boldsymbol{x}} = \boldsymbol{F}(t)\delta\boldsymbol{x} + \boldsymbol{G}(t)\boldsymbol{w}, \tag{30}$$

where the Jacobian matrices $\boldsymbol{F}$ and $\boldsymbol{G}$, and the process covariance matrix $\boldsymbol{\mathcal{Q}}$ based on the process noise $\boldsymbol{w}$ are given in the Appendix A of Okuhara et al. (2022).

4.2 Measurement model (mode 1)

When GNSS measurements are available, GNSS aids the INS, and the calibration of the PARS ground antenna mounting presented in Okuhara et al. (2021) is performed using the position estimate from the GNSS-aided INS as ground truth.

GNSS. The GNSS measures the position of the UAV in the $\{e\}$-frame. The measurement can be expressed as

$$\boldsymbol{y}^e_{\text{gnss}} = \boldsymbol{p}^e_{\text{gnss}} + \varepsilon_{\text{gnss}}, \tag{31}$$

and the measurement estimate becomes

$$\hat{\boldsymbol{y}}^e_{\text{gnss}} = \hat{\boldsymbol{p}}^e_{eb}. \tag{32}$$

Therefore, the measurement matrix is trivially

$$\boldsymbol{H}_{\text{gnss}} = (\boldsymbol{I}_3\ \boldsymbol{0}_{3\times15}) \in \mathbb{R}^{3\times18}. \tag{33}$$

The measurement covariance matrix is given as

$$\boldsymbol{\mathcal{R}}^e_{\text{gnss}} = \hat{\boldsymbol{R}}_{en}\text{diag}(\mathbb{E}[\varepsilon^2_{\text{gnss},N}], \mathbb{E}[\varepsilon^2_{\text{gnss},E}], \mathbb{E}[\varepsilon^2_{\text{gnss},D}])\hat{\boldsymbol{R}}^\intercal_{en}. \tag{34}$$

where N, E and D represents the NED components, respectively. $\hat{\boldsymbol{R}}_{en}$ is calculated based on the position $\hat{\boldsymbol{p}}^e_{eb}$ via estimated latitude, $\hat{\mu}$, and longitude, $\hat{\lambda}$.

PARS: Calibration. As mentioned in Albrektsen et al. (2017), the elevation angle is very uncertain due to multipath errors. To mitigate the noise in the PARS elevation angle, the vertical measurement in (15) was replaced by an exogenous altitude measurement from a barometric sensor:

$$\gamma_{\text{alt}} = (0\ 0\ 1)\,\boldsymbol{p}^n_{rb} + b_{\text{alt}} + \varepsilon_{\text{alt}} \tag{35}$$

where b^n_{alt} is the barometer altitude bias. The PARS range was also modified by the barometric measurement

$$\bar{\rho}_y = \sqrt{\rho^2_y - \gamma^2_{\text{alt}}}, \tag{36}$$

such that only the horizontal range and the azimuth angle are used to update the horizontal position, preventing the noise in elevation angle measurement from affecting INS aiding altogether. The resulting Cartesian position measurement becomes

$$\boldsymbol{p}^r_{\text{PARS,alt}} = \begin{pmatrix} \bar{\rho}_y \cos\psi_y \\ \bar{\rho}_y \sin\psi_y \\ \gamma_{\text{alt}} \end{pmatrix}. \tag{37}$$

The calibration measurement model is then given as

$$\underbrace{\hat{\boldsymbol{R}}_{nr}\boldsymbol{p}^r_{rb}}_{\boldsymbol{y}_{\text{pars}}} = \underbrace{\hat{\boldsymbol{R}}^\intercal_{en}\,(\hat{\boldsymbol{p}}^e_{eb} - \boldsymbol{p}^e_{er})}_{\hat{\boldsymbol{y}}_{\text{pars}}} + \underbrace{\hat{\boldsymbol{R}}^\intercal_{en}}_{\boldsymbol{H}_{\text{pos}}}\delta\boldsymbol{p} + \underbrace{\hat{\boldsymbol{R}}_{nr}\boldsymbol{S}\,(\boldsymbol{p}^r_{rb})}_{\boldsymbol{H}_{\text{calib}}}\delta\boldsymbol{a}^n_r \tag{38}$$

where the measurement, the measurement estimate, and the measurement matrices are respectively

$$\boldsymbol{y}^n_{\text{pars}} = \hat{\boldsymbol{R}}_{nr}\boldsymbol{p}^r_{\text{PARS,alt}}, \tag{39}$$

$$\hat{\boldsymbol{y}}^n_{\text{pars}} = \boldsymbol{R}^\intercal_{en}\,(\hat{\boldsymbol{p}}^e_{eb} - \boldsymbol{p}^e_{er})\,, \tag{40}$$

$$\boldsymbol{H}_{\text{pos}} = \hat{\boldsymbol{R}}^\intercal_{en}, \tag{41}$$

$$\boldsymbol{H}_{\text{calib}} = \hat{\boldsymbol{R}}_{nr}\boldsymbol{S}\left(\hat{\boldsymbol{R}}^\intercal_{er}\,(\hat{\boldsymbol{p}}^e_{eb} - \boldsymbol{p}^e_{er})\right), \tag{42}$$

and the resulting measurement matrix becomes

$$\boldsymbol{H}_{\text{pars}} = (\boldsymbol{H}_{\text{pos}}\ \boldsymbol{0}_{3\times12}\ \boldsymbol{H}_{\text{calib}}) \in \mathbb{R}^{3\times18}. \tag{43}$$

Here, $\hat{\boldsymbol{p}}^e_{eb}$ is the UAV position estimate from the aided INS, and $\boldsymbol{p}^r_{rb}$ is the PARS UAV position (i.e. $\boldsymbol{p}^r_{\text{PARS,alt}}$). $\boldsymbol{p}^e_{er}$ is the ground station position and is considered to be known since it can be surveyed in advance of flights. The derivation of (38) can be found in Appendix B of Okuhara et al. (2022).

Furthermore, the covariance of the original PARS-altitude measurement ρ_y, ψ_y and γ_{alt} is

$$\boldsymbol{\mathcal{R}}_{\text{PARS,alt}} = \text{diag}(\mathbb{E}[\varepsilon^2_\rho], \mathbb{E}[\varepsilon^2_\psi], \mathbb{E}[\varepsilon^2_{\text{alt}}]). \tag{44}$$

$\boldsymbol{\mathcal{R}}_{\text{PARS,alt}}$ given in cylindrical coordinates needs to be converted to $\boldsymbol{\mathcal{R}}^r_{\text{PARS,alt}}$ in Cartesian coordinates, then be transformed from $\{r\}$-frame to $\{n\}$-frame, as (39)–(43) are in the $\{n\}$-frame. Okuhara et al. (2021) and Okuhara et al. (2022) provide further details about the computation of the covariance matrix.

4.3 Measurement model (mode 2)

When GNSS is unavailable, PARS and barometer aid the INS in the horizontal and vertical directions, respectively. Unlike Sec. 4.2.2, the barometer altitude as a replacement for the PARS vertical component was treated separately from the PARS measurements to include the effect of the Earth's curvature.

PARS. In Okuhara et al. (2022), the horizontal range, $\bar{\rho}_y$, was computed by approximating the elevation angle (α) using a trigonometric relation. However, this paper does not use this method, as the trigonometric approximation is not very accurate when the UAV is close to the PARS ground antenna. Instead, the horizontal range ($\bar{\rho}_y$) was computed in a similar manner with (36) using barometric altitude.

The horizontal components of Cartesian PARS position measurements can be expressed as

$$\boldsymbol{y}^r_{\text{PARS}} = \begin{pmatrix} \bar{\rho}_y \cos\psi_y \\ \bar{\rho}_y \sin\psi_y \end{pmatrix}. \tag{45}$$

The measurement estimate is given as

$$\hat{\boldsymbol{y}}^r_{\text{PARS}} = \underbrace{\begin{pmatrix} 1 & 0 & 0 \\ 0 & 1 & 0 \end{pmatrix}}_{\boldsymbol{\Pi}} \underbrace{\hat{\boldsymbol{R}}^\intercal_{nr}\boldsymbol{R}^\intercal_{en}}_{\hat{\boldsymbol{R}}^\intercal_{er}} (\hat{\boldsymbol{p}}^e_{eb} - \boldsymbol{p}^e_{er})\,. \tag{46}$$

Hence, the measurement matrix becomes

$$\boldsymbol{H}_{\text{PARS}} = (\boldsymbol{\Pi}\hat{\boldsymbol{R}}^\intercal_{er}\ \boldsymbol{0}_{2\times15}) \in \mathbb{R}^{2\times18}. \tag{47}$$

The covariance of the PARS measurement ρ_y and ψ_y is

$$\boldsymbol{\mathcal{R}}_{\text{PARS}} = \text{diag}(\mathbb{E}[\varepsilon_\rho^2], \mathbb{E}[\varepsilon_\psi^2]). \tag{48}$$

Similarly to (44), $\boldsymbol{\mathcal{R}}_{\text{PARS}}$ needs to be converted from cylindrical coordinates to Cartesian coordinates. Please see Okuhara et al. (2022) for details.

Barometer. A barometer measures the altitude from the reference surface:

$$\boldsymbol{y}_{\text{alt}}^n = \gamma_{\text{alt}}. \tag{49}$$

The measurement estimate can be computed from the position estimate using

$$\hat{\boldsymbol{y}}_{\text{alt}}^n = \underbrace{(0\ 0\ 1)}_{\boldsymbol{C}} \hat{\boldsymbol{R}}_{en}^\intercal \left(\hat{\boldsymbol{p}}_{eb}^e - \boldsymbol{p}_{er}^e\right), \tag{50}$$

and hence

$$\boldsymbol{H}_{\text{alt}} = (\boldsymbol{C}\hat{\boldsymbol{R}}_{en}^\intercal\ \boldsymbol{0}_{1\times 15}) \in \mathbb{R}^{1\times 18}. \tag{51}$$

The measurement covariance matrix is trivially

$$\boldsymbol{\mathcal{R}}_{\text{alt}} = \mathbb{E}[\varepsilon_{\text{alt}}^2]. \tag{52}$$

5. RESULTS AND DISCUSSION

We conducted two independent field tests on the 28$^{\text{th}}$ November 2019 at Raudstein in the north of Agdenes outside Trondheim and on the 20$^{\text{th}}$ September 2022 at Bleik in northern Norway. Fig. 3 indicates the flight paths with ground antenna positions. We performed test flights using a Skywalker X8 UAV with a single PARS ground antenna and recorded IMU, RTK-GNSS, and PARS measurements with corresponding timestamps in addition to multiple sensor measurements (including a barometer) from a Pixhawk autopilot. Before conducting the flights, we measured the PARS ground antenna's position and orientation by GNSS and a compass. See Gryte et al. (2020) for more details about the equipment on the payload and the ground station.

The navigation system presented in this paper was implemented in DUNE unified navigation environment (Pinto et al., 2013) for real-time operation in the fields. The presented algorithm was written in C++ using the mathematical libraries provided by DUNE.

The implementation in DUNE was verified using the replay data obtained from the field tests.

The numerical values for process and measurement covariance matrices $\boldsymbol{\mathcal{Q}}$ and $\boldsymbol{R}_\star$ (i.e. $\varepsilon_\star \sim \mathcal{N}(0, \sigma_\star^2)$) are found in the Appendix C of Okuhara et al. (2022).

5.1 Calibration of ground antenna orientation

The initial estimate of the ground antenna orientation was assumed to contain $\pm 10^\circ$ error

$$\boldsymbol{\Theta}_{\text{PARS}_R} = (\phi_r\,, \theta_r\,, \psi_r) = (0^\circ\,, 0^\circ\,, -116^\circ) \tag{53}$$

$$\boldsymbol{\Theta}_{\text{PARS}_B} = (\phi_a\,, \theta_a\,, \psi_a) = (0^\circ\,, 0^\circ\,, -47^\circ), \tag{54}$$

where the subscript R and B denote Raudstein and Bleik locations, respectively.

The calibration mode (i.e. mode 1) was enabled in the middle of the flight, approximately for 150 s. In other words, our navigation system (aided-INS) used mode 2 from the start of the flight and switched to mode 1, then switched back to mode 2 after the calibration mode is disabled 150 s later.

Figs. 4–5 present the results of the in-flight calibration operation, for Raudstein and Bleik respectively. Fig. 4a and Fig. 5a show that the ground antenna orientation was estimated successfully and converged to $+10^\circ$ in the yaw angle. In Fig. 4b and Fig. 5b, the NED position estimate from the aided-INS is compared to the RTK-GNSS as ground-truth. In the North and East direction, the dotted blue line (the aided-INS) shifts to match the dotted orange line (RTK-GNSS) after the calibration starts. The 2D plot in Fig. 4c and 5c shows the improvement in the position estimate more clearly. In the Down direction, except for the calibration period, the dotted blue line (the aided-INS) is shifted from the dotted orange line (RTK-GNSS) due to the bias in the barometer altitude. During the calibration, as the RTK-GNSS is aiding the INS, the Down position matches with the ground truth. In Fig. 4d and Fig. 5d, the NED position error significantly improved in the North and East directions.

To ensure safety in shared airspace, it is important that the vertical bias does not propagate in the horizontal bias. However, in the current formulation, the bias in the altitude measurement affects the horizontal position estimate through the horizontal range computation in (36). As the bias in the barometer altitude changes depending on the altitude, it is difficult to compensate by a fixed offset. For a better estimate of barometer bias, we need a smarter algorithm.

5.2 Approximate mounting

In addition to the situation considered in Sec. 5.1 with in-flight calibration, we also considered a situation in which the aided-INS uses a fixed approximate ground antenna mounting with $\pm 1^\circ$ error throughout the entire flight without calibration. We used the Raudstein replay data and the same initial angle, as in Gryte et al. (2020):

$$\boldsymbol{\Theta}_{\text{PARS}_R} = (0^\circ,\ 0^\circ,\ -106^\circ).$$

where this paper propagated the system dynamics in the ECEF frame, while Gryte et al. (2020) used the local NED frame.

Fig. 6 shows the result from the approximate mounting. The NED position error plot in Fig. 6a can be compared with Fig.15 in Gryte et al. (2020). In the North and East direction, the position error plots behave similarly. However, in the Down direction, the error plot in Fig.15 in Gryte et al. (2020) has a clear inclination as the distance from the ground antenna increases, while Fig. 6a does not. Since the barometer measures altitude from the reference surface perpendicular to the tangent line of the earth curvature, using the barometer altitude directly in the local NED frame induces errors as explained in Gryte et al. (2020). Although the use of the ECEF frame could solve this issue, the position estimate in the Down direction has a slightly larger mean error (considering barometer altitude bias by approximately 10 m).

6. CONCLUSION

In this paper, the previously presented in-flight calibration algorithm which estimates the ground antenna orientation

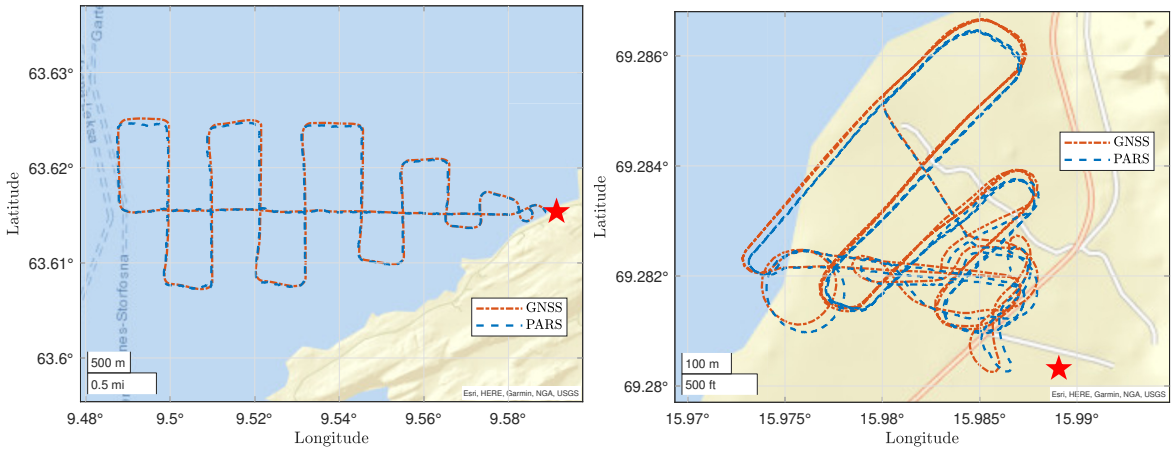

(a) Raudstein (b) Bleik

Fig. 3. Flight path of the UAV with ground antenna positions indicated

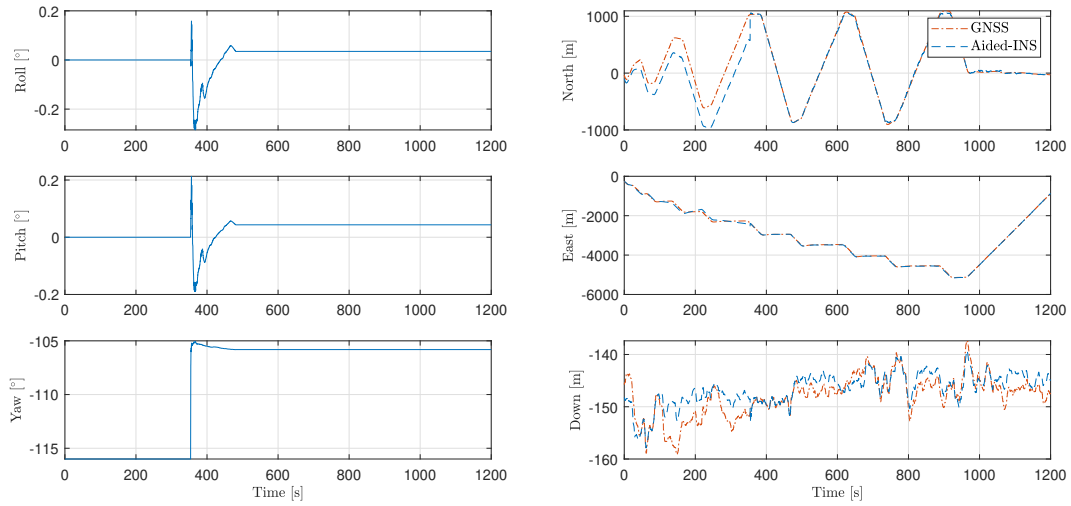

(a) Attitude of the ground antenna (b) NED position with RTK-GNSS reference in 1D

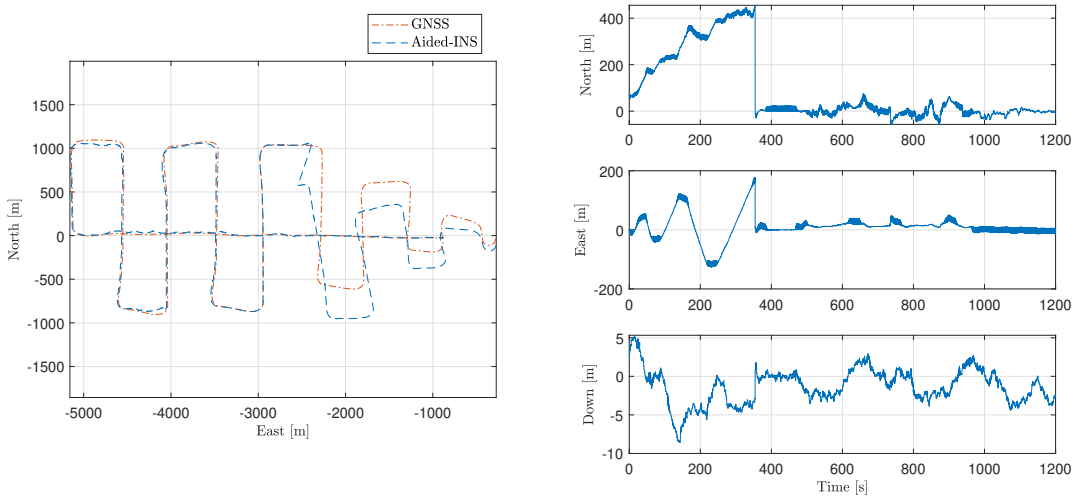

(c) NE position with RTK-GNSS reference in 2D (d) NED position error w.r.t RTK-GNSS reference

Fig. 4. Calibrated mounting (Raudstein)

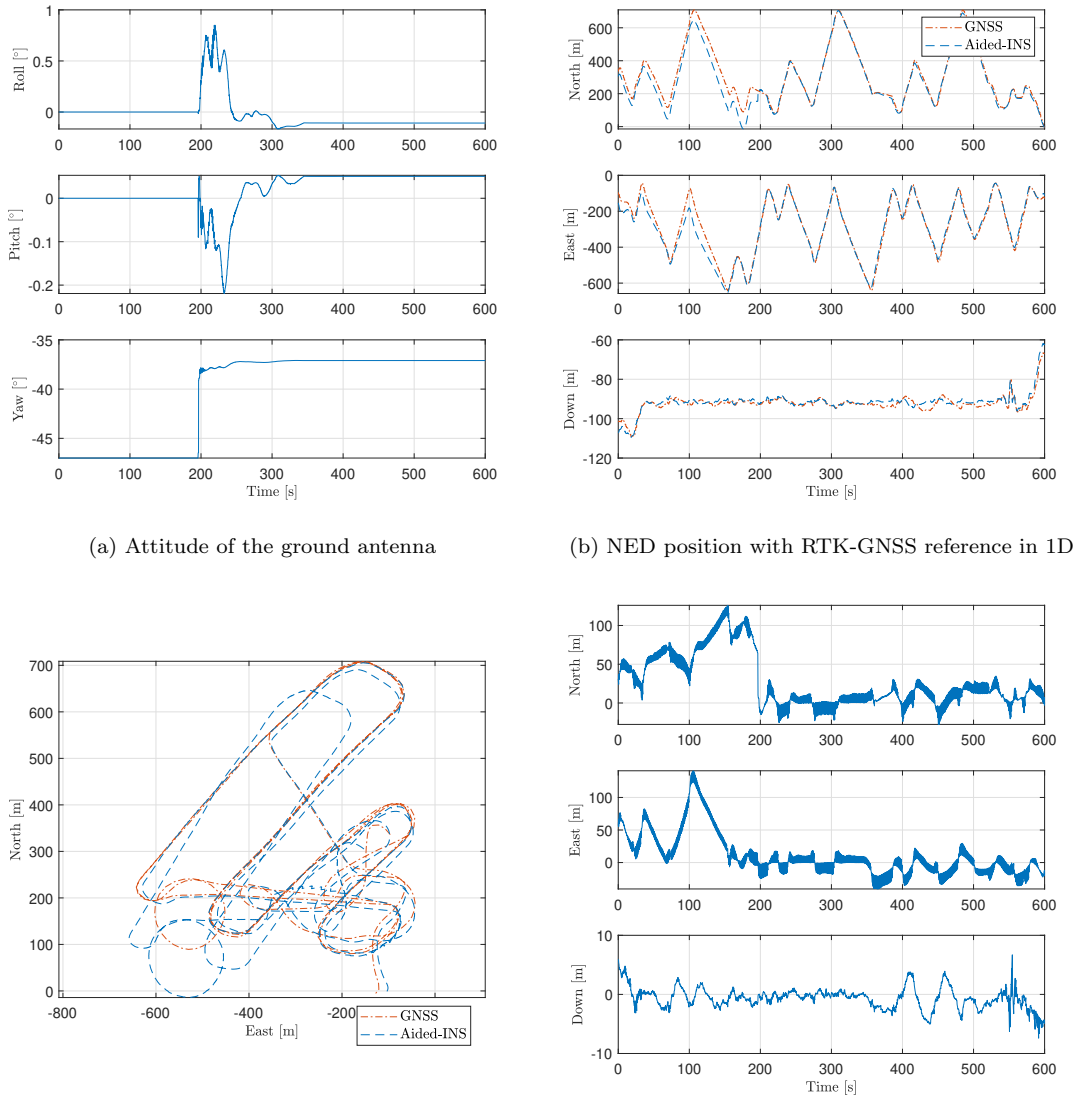

(a) Attitude of the ground antenna

(b) NED position with RTK-GNSS reference in 1D

(c) NE position with RTK-GNSS reference in 2D

(d) NED position error w.r.t RTK-GNSS reference

Fig. 5. Calibrated mounting (Bleik)

for the phased array radio system (PARS) was implemented in DUNE unified navigation environment for real-time operation. The algorithm is integrated with the aided-inertial navigation system (aided-INS), and the INS equations are propagated in the Earth Fixed Earth Centred (ECEF) frame, while the previous implementation used the local North East Down (NED) frame. We conducted field tests using a single ground antenna at Raudstein and Bleik to collect replay data to validate the implementation. The recorded replay data included IMU, RTK-GNSS, PARS, and Pixhawk autopilot (with barometer) measurements. The estimates from the implemented navigation system were verified by comparing them with RTK-GNSS measurements and Pixhawk autopilot solutions as ground truth.

The calibration mode was enabled for approximately 150 s in the middle of the flights, and the position estimate improved significantly after the calibration by estimating the precise orientation of the ground antenna. In addition, the result showed that the propagation of navigation equations in the ECEF frame, instead of the local NED frame, is beneficial to overcome the error induced in the vertical position estimate presented previously.

In future work, we want to add barometer bias estimation to the implementation, and conduct flights in the fields using the navigation solutions from DUNE in the control loop of the autopilot.

REFERENCES

Albrektsen, S.M., Bryne, T.H., and Johansen, T.A. (2018a). Phased array radio system aided inertial navigation for unmanned aerial vehicles. In *Proc. of the IEEE Aerospace Conference*, 1–11. Big Sky, Montana.

Albrektsen, S.M., Bryne, T.H., and Johansen, T.A. (2018b). Robust and secure uav navigation using gnss, phased-array radiosystem and inertial sensor fusion. In

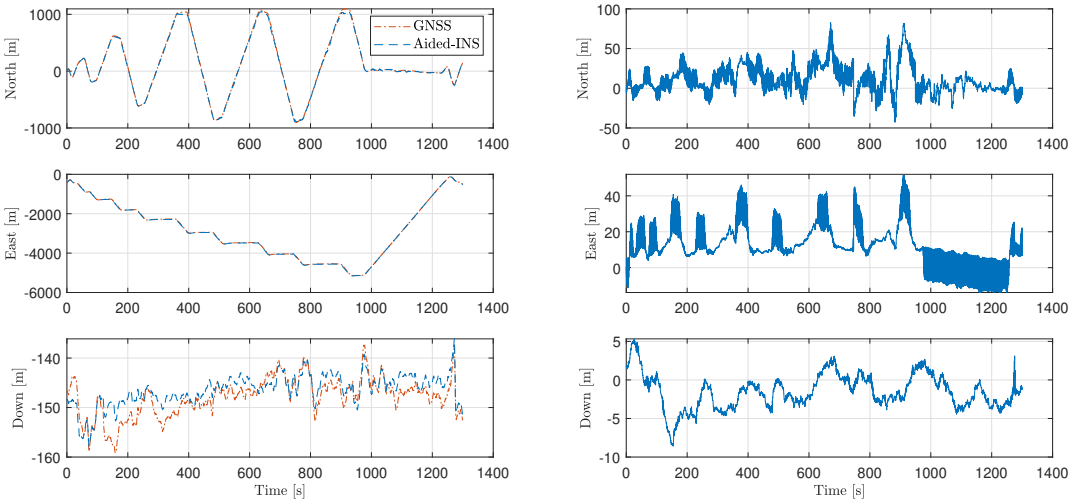

(a) NED position with RTK-GNSS reference in 1D

(b) NED position error w.r.t RTK-GNSS reference

Fig. 6. Approximate mounting (Raudstein)

2nd IEEE Conference on Control Technology and Applications, 1338–1345. Copenhagen, Denmark.

Albrektsen, S.M., Sœgrov, A., and Johansen, T.A. (2017). Navigation of uav using phased array radio. In *Workshop on Research, Education and Development of Unmanned Aerial Systems (RED UAS)*, 138–143.

Farrell, J.A. (2008). *Aided Navigation: GPS with High Rate Sensors*. McGraw-Hill, Inc., Maidenhead, 1 edition.

Groves, P.D. (2013). *Principles of GNSS, Inertial, and Multisensor Integrated Navigation Systems*. Artech House, 2nd edition.

Gryte, K., Bryne, T.H., Albrektsen, S.M., and Johansen, T.A. (2019). Field test results of gnss-denied inertial navigation aided by phased-array radio systems for uavs. In *2019 International Conference on Unmanned Aircraft Systems (ICUAS)*, 1398–1406.

Gryte, K., Bryne, T.H., and Johansen, T.A. (2020). Unmanned aircraft flight control aided by phased-array radio navigation. *Journal of Field Robotics*, 1–20.

Humphreys, T. (2017). Interference. In P.J. Teunissen and O. Montenbruck (eds.), *Springer Handbook of Global Navigation Satellite Systems*, Springer Handbooks. Springer Cham. doi:10.1007/978-3-319-42928-1.

Kerns, A.J., Shepard, D.P., Bhatti, J.A., and Humphreys, T.E. (2014). Unmanned aircraft capture and control via GPS spoofing. *Journal of Field Robotics*, 31(4), 617–636.

Markley, F.L. (2003). Attitude error representation for kalman filtering. *Journal of Guidance, Control, and Dynamics*, 26(2), 311–317.

Okuhara, M., Gryte, K., Bryne, T.H., and Johansen, T.A. (2022). Phased array radio navigation system on uavs: In-flight re-calibration. *TechRxiv*. doi: 10.36227/techrxiv.20337084.v1.

Okuhara, M., Bryne, T.H., Gryte, K., and Johansen, T.A. (2021). Phased array radio navigation system on uavs: Gnss-based calibration in the field. In *2021 International Conference on Unmanned Aircraft Systems (ICUAS)*, 210–218.

Pinker, A. and Smith, C. (1999). Vulnerability of the GPS signal to jamming. *GPS Solutions*, 3(2), 19–27.

Pinto, J., Dias, P.S., Martins, R., Fortuna, J., Marques, E., and Sousa, J. (2013). The lsts toolchain for networked vehicle systems. In *2013 MTS/IEEE OCEANS-Bergen*, 1–9. IEEE.

Solà, J. (2017). Quaternion kinematics for the error-state kalman filter.